

Electrodeposited Zn–TiO₂ nanocomposite coatings and their corrosion behavior

Adriana Vlasa · Simona Varvara · Aurel Pop · Caius Bulea · Liana Maria Muresan

Received: 26 August 2009 / Accepted: 27 March 2010 / Published online: 13 April 2010
© Springer Science+Business Media B.V. 2010

Abstract The present paper aims to investigate the electrodeposition on steel substrate and the corrosion behavior of Zn–TiO₂ nanocomposite coatings. Zn–TiO₂ composite coatings were electrodeposited on OL 37 steel from an electrolyte containing ZnCl₂, KCl, HBO₃ (pH 5.7) brightening agents and dispersed nanosized TiO₂. Corrosion measurements were performed in 0.2 g L⁻¹ (NH₄)₂SO₄ solution (pH 3) by using electrochemical methods (open-circuit potential measurements, polarization curves, electrochemical impedance spectroscopy). The results of electrochemical measurements were corroborated with those obtained by using non-electrochemical methods (X-ray diffraction, atomic force microscopy and scanning electron microscopy). The results indicate that the composite coatings exhibit higher corrosion resistance as compared to pure Zn coatings and a non-linear dependence of their polarization resistance on TiO₂ concentration in the plating bath was found. The importance of TiO₂ nature and concentration regarding the properties of the composite coatings was demonstrated.

Keywords Zn–TiO₂ composite coatings · Electrolytic co-deposition · Corrosion · Nanoparticles

1 Introduction

Zinc has found widespread use as the basis of a whole range of sacrificial coatings for ferrous substrates. Compared to zinc plating, zinc composites provide superior mechanical properties and better sacrificial protection to steel, since they corrode slower than pure zinc. Therefore, the interest for zinc composites has increased lately, due to their excellent mechanical and tribological properties, and due to their improved corrosion resistance and paint ability [1].

Electrodeposition techniques have provided a route to many new composite coatings with metallic matrix [2]. Using these methods, a variety of nanosized particles (typically with spherical shape), ranging from 4 to 800 nm diameters, have been successfully incorporated into zinc deposits. These include silicon dioxide (SiO₂) [1, 3] titanium dioxide (TiO₂) [4–6] and aluminum oxide (Al₂O₃) [7, 8].

Among the nanomaterials, TiO₂ is in great choice for the generation of composite zinc coatings on steel, due to its increasing availability and to the fact that TiO₂ can reinforce zinc electroplate to improve corrosion and wear resistance, hardness and other properties such as magnetic and photocatalytic properties, lubricity etc. [3]. TiO₂ micron or submicron size particles co-deposition with Zn usually takes place in a classical zinc electroplating bath containing suspended TiO₂ particles [6, 9, 10]. A lot of parameters, such as current profile, bath composition, pH, particle concentration, temperature, stirring rate, presence of additives etc., strongly influence the properties of the

A. Vlasa · L. M. Muresan (✉)
Department of Physical Chemistry, “Babes-Bolyai” University,
11 Arany Janos St., 400028 Cluj-Napoca, Romania
e-mail: limur@chem.ubbcluj.ro

S. Varvara
Department of Topography, “1 Decembrie 1918” University,
11–13 Nicolae Iorga St., 510009 Alba-Iulia, Romania

A. Pop
Department of Physics, “Babes-Bolyai” University, 11 Arany
Janos St., 400028 Cluj-Napoca, Romania

C. Bulea
BETAK S.A, 4 Industriei St., 420063 Bistrita, Romania

resulting composite coatings [2]. However, due to the complexity of the process, there are still many unknown aspects to be considered.

In this context, the aim of this work is to investigate the influence of the nature and concentration of TiO_2 nanoparticles on the corrosion resistance of Zn– TiO_2 composite films plated on steel substrate. The results of electrochemical measurements (open-circuit potential, polarization curves, electrochemical impedance spectroscopy) were corroborated with those obtained by using non-electrochemical methods (X-ray diffraction, atomic force microscopy, scanning electron microscopy).

2 Experimental details

2.1 Materials

Two types of TiO_2 nanoparticles [Alfa Aesar (AA) 99.9%, 32 nm, anatase and Degussa (D) 99.5%, 21 nm mixture of rutile and anatase] were suspended in an aqueous electrolyte ($\text{pH } 5.7$) containing 75 g L^{-1} ZnCl_2 , 230 g L^{-1} KCl , 20 g L^{-1} H_3BO_3 and two brightening agents in a concentration of 1 mL L^{-1} each. The concentrations of TiO_2 nanoparticles in the plating bath were 3, 5 and 10 g L^{-1} , respectively.

For corrosion studies, a solution of 0.2 g L^{-1} $(\text{NH}_4)_2\text{SO}_4$ (Riedel-de Haën, Germany) ($\text{pH } 3$) was used. All other reagents were analytical grade and used as received.

2.2 Electrodes preparation

The electrodeposition of the Zn– TiO_2 nanocomposite films was carried out in a two compartments glass cell, with the capacity of 250 mL, using a steel (OL37) disk electrode ($\varnothing = 0.8 \text{ cm}$) as working electrode, a $\text{Ag}/\text{AgCl}/\text{KCl}_{\text{sat}}$ as reference electrode and a Pt foil as counter electrode. Before electrodeposition, the working electrode was wet polished on emery paper of different granulations and finally on felt with a suspension of alumina. Before plating, the electrode was ultrasonicated during 2 min, washed with acetone and distilled water in order to remove the impurities from the surface.

The approximately $50 \mu\text{m}$ thick composite coatings were obtained at a constant current density ($i = 20 \text{ mA cm}^{-2}$) by using a potentiostat/galvanostat (Votlab PGP201, Radiometer analytical), during 30 min, at room temperature ($25 \pm 2^\circ\text{C}$). The TiO_2 nanoparticles were maintained in suspension by using a magnetic stirrer (stirring rate, 200 rpm). The resulting electrodes were named $\text{Zn-3 g L}^{-1} \text{ TiO}_2$, $\text{Zn-5 g L}^{-1} \text{ TiO}_2$ and $\text{Zn-10 g L}^{-1} \text{ TiO}_2$, respectively.

2.3 Corrosion measurements

The corrosion measurements (open-circuit potential, polarization curves) were performed with a potentiostat Autolab-PGSTAT 10, (Eco Chemie BV, Utrecht, Netherlands). Before the impedance and polarization measurements, the open-circuit potential (OCP) was recorded during 1 h, until it was stabilized. The impedance experiments were carried out at the open-circuit potential by using a BioLogic potentiostat SP-150 (Claix, France), in the frequency range 100 kHz–100 MHz at five points per hertz decade with an AC voltage amplitude of $\pm 10 \text{ mV}$. The impedance data were then analyzed with software based on a Simplex parameter regression.

2.4 Morphological and structural analysis

The morphological and structural analysis of the coatings were performed by using X-ray diffraction (XRD) method on a Bruckner type diffractometer. A Philips XL-30 Scanning Electron Microscope (SEM) coupled with an energy-dispersive X-ray (EDX) system EDAX NEW XL30 was used for morphological analysis and composition determination of the coatings. Topographic analysis of the surface were performed by using an Atomic Force Microscope (AFM Solver).

3 Results and discussion

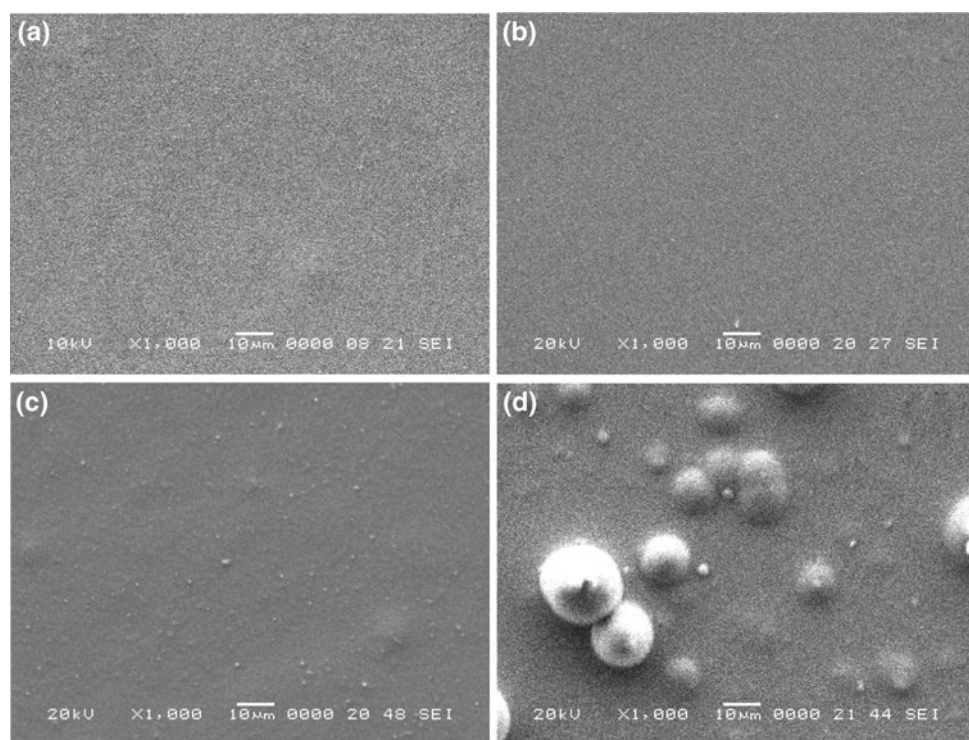
3.1 Morphological and structural analysis

Figure 1 presents the surface morphology of pure zinc and of Zn– TiO_2 Degussa coatings, before the corrosion measurements.

As it can be observed, the embedded TiO_2 nanoparticles change the structure of the metal deposit, which becomes more fine-grained, because the nanoparticles provide more nucleation sites and retard the crystal growth. The surface morphology does not change significantly by changing the type of the TiO_2 nanoparticles (D or AA), if their concentration in the plating bath is the same. It should be mentioned that by increasing the TiO_2 concentration in the plating bath, the nanoparticles show a distinct tendency to form conglomerates in solution due to their high surface energy and to the more intense interactions between the particles [5]. These conglomerates are incorporated and distributed all over the electrode surface (Fig. 1c, d) and their dimensions increase from $1 \mu\text{m}$ for the sample $\text{Zn-3 g L}^{-1} \text{ TiO}_2$ to $15 \mu\text{m}$ for the coating $\text{Zn-10 g L}^{-1} \text{ TiO}_2$.

A possible co-deposition mechanism is that suggested by Guglielmi [11] and confirmed by other authors [12]. This two-step mechanism postulates a weak adsorption

Fig. 1 SEM micrographs of the surface of Zn (**a**), and Zn–TiO₂ films prepared with 3 g L⁻¹ (**b**), and 5 g L⁻¹ (**c**), and 10 g L⁻¹ (**d**), Degussa nanoparticles



with an essentially physical character of TiO₂ nanoparticles on the electrode surface, followed by a strong field-assisted adsorption of the particles carrying a positive charge, due to the adsorption of Zn²⁺ ions on their surface. Once the particles are adsorbed, they are entrapped in the growing metallic deposit. At high TiO₂ concentrations, the particles agglomerate and a decreasing incorporation trend is noticed.

The TiO₂ presence in the nanocomposite coatings was determined by EDX analysis. In the case of Zn-3 g L⁻¹ TiO₂ (D), due to a very poor incorporation fraction, below the sensibility of the system, the presence of Ti could not be shown. On the contrary, in the case of the deposits obtained with 5 g L⁻¹ in the plating bath, the EDX spectra clearly revealed the presence of Ti in addition to an increase of the oxygen content, indicating the presence of TiO₂ nanoparticles in the zinc matrix (Fig. 2). The TiO₂ content in the deposit is relatively weak (0.47 weight % Ti corresponding to 0.79 weight % TiO₂), but the results are similar to those reported in the literature for metal-nano-particles composite coatings [2].

The presence of TiO₂ diffraction lines in the X-ray spectra of the deposits (Fig. 3) confirmed also the formation of the Zn–TiO₂ composite layers. The analysis of diffractograms shows that the composition of the plating bath has a strong influence on the crystal orientation in the deposit. Thus, the diffraction maximum (101) of Zn in the composite layers decreases, while the (100) maximum

increases. These results are in accordance with those stated in the literature, that the particles embedded in the coatings can affect the preferred orientation of the metallic matrix as a consequence of changes on the metal deposition mechanism [13].

Although the XRD peaks are narrow, the grain size of the metallic matrix was estimated from the width of (110) diffraction line. Thus, the grain size of the composite deposits was proved to be smaller (19.89 nm for Zn-5 g L⁻¹ TiO₂, 19.14 nm for Zn-10 g L⁻¹ TiO₂) than that of the pure Zn coatings (20.35 nm). Even if the change in grain size is not obvious, the decreasing tendency can be related to a modification of the competition between nucleation and crystals growth in the presence of TiO₂. The nanoparticles enhance nucleation by creating disorder in the incorporation of adatoms into the lattice or inhibit surface diffusion of adatoms towards growing centers and exert a detrimental effect on the crystal growth. Similar results were reported for deposition of zinc with TiO₂ nanoparticles from sulfate-based electrolytes [13].

The topographic images of the surface obtained by AFM measurements for composite coatings obtained from solutions containing different concentrations of TiO₂ (D) (Fig. 4) suggest a non-linear dependence of the deposit uniformity on TiO₂ concentration in the plating bath. Thus, in the case of 5 g L⁻¹ TiO₂ (Fig. 4b), the cathodic deposit is much more uniform than in the case when 0 g L⁻¹ (Fig. 4a) or 10 g L⁻¹ TiO₂ (Fig. 4c) were used.

Fig. 2 EDX spectra of composite coating Zn–TiO₂ (5 g L⁻¹ TiO₂ Degussa in the plating bath) deposited on OL37 steel

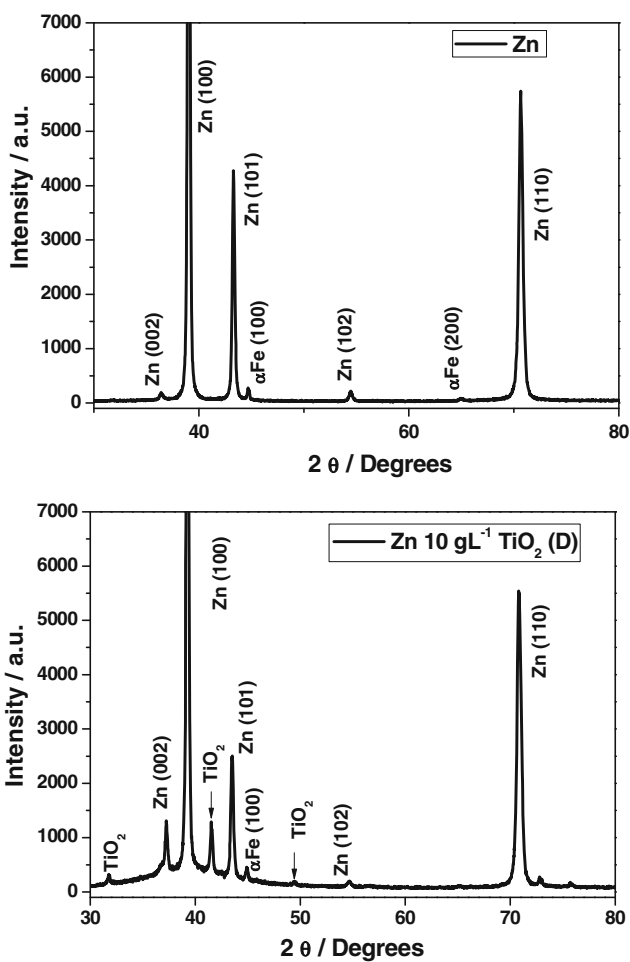
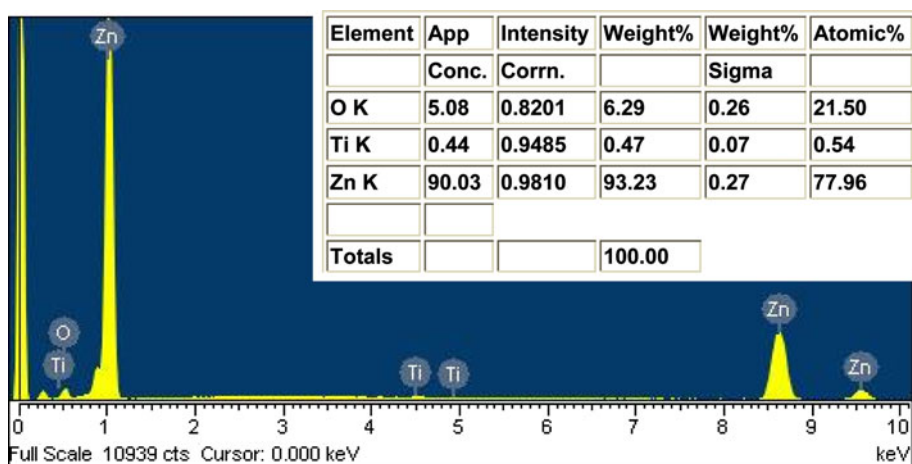


Fig. 3 XRD spectra of Zn and Zn–TiO₂ deposits

Figure 5 presents the surface morphology of pure zinc and of Zn–TiO₂ Degussa coatings after 48 h immersions in the (NH₄)₂SO₄ (pH 3) corrosive media.

As expected, after a 48 h immersion in the corrosive solution, the pure Zn coating appears to be covered with corrosion products on the whole surface, indicating that

generalized corrosion occurs (Fig. 5a). The presence of TiO₂ (D) nanoparticles embedded in the zinc matrix makes the composite coatings more corrosion-resistant, but their beneficial effect upon the deposit quality appears to be strongly dependent on the degree of TiO₂ incorporation in the metallic coatings. Thus, the poor corrosion resistance observed in the case of Zn-3 g L⁻¹ TiO₂ (D) coating (Fig. 5b) is probably a result of the small incorporation fraction of TiO₂ nanoparticles in the metallic deposit, too small to be evidenced by EDX and XRD measurements. It is even possible that the embedded nanoparticles disturb the electrocrystallization process, by generating dislocations and defects in the metallic matrix, which act as chemical heterogeneities and locally favor the corrosion process.

On contrary, the Zn–TiO₂ coatings prepared with higher concentrations of Degussa nanoparticles (5, 10 g L⁻¹) show a much better corrosion resistance (Fig. 5c, d). However, it should be noticed that the surface of the Zn coating incorporating 5 g L⁻¹ TiO₂ (D) is almost not affected by corrosion after 48 h of immersion in the corrosive solution (Fig. 5c), while Zn-10 g L⁻¹ TiO₂ coatings are covered in a certain degree with corrosion products. This behaviour confirms the assumption that in the investigated experimental conditions the optimum concentration of the TiO₂ (D) nanoparticles in the plating bath is 5 g L⁻¹. Consequently, electrochemical investigations of the corrosion process were carried out only with Zn-5 g L⁻¹ TiO₂ and Zn-10 g L⁻¹ TiO₂ electrodes.

3.2 Polarization curves

In order to correlate the Zn–TiO₂ deposits quality with their corrosion resistance, electrochemical measurements were carried out.

The cathodic and anodic polarization behavior of pure zinc and Zn–TiO₂ coatings recorded after 1 h exposure in (NH₄)₂SO₄ (pH 3) corrosive media are presented in Fig. 6.

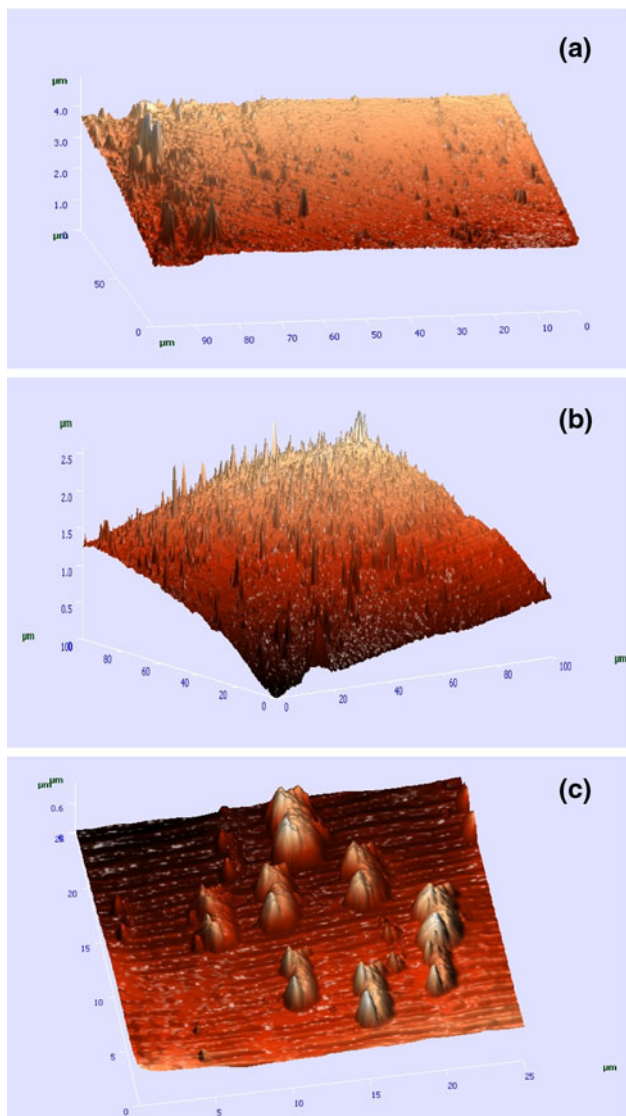


Fig. 4 3D images for Zn (scanned area $4 \times 100 \times 100 \mu\text{m}$) (a), Zn–TiO₂ coating electrodeposited from a bath containing 5 g L^{-1} TiO₂ (D), (scanned area $2.5 \times 100 \times 100 \mu\text{m}$) (b) and for Zn–TiO₂ coating electrodeposited from a bath containing 10 g L^{-1} TiO₂ (D), (scanned area $0.6 \times 25 \times 25 \mu\text{m}$) (c)

In the close vicinity of the open-circuit corrosion potential, according to the Stern-Gear theory [14] the current density i is expressed by the following equation:

$$i = i_{corr} \{ \exp[b_a(E - E_{corr})] - \exp[b_c(E - E_{corr})] \} \quad (1)$$

where b_a and b_c are the anodic and cathodic activation coefficients, respectively. Therefore, the values of E_{corr} and the corrosion current density, i_{corr} were evaluated from non-linear regression calculation near zero overall current.

The values of the corrosion kinetic parameters obtained in the absence and in the presence of the two different types of TiO₂ nanoparticles embedded in the zinc deposit are

presented in Table 1. In all cases, the high values of the correlation factor R^2 indicate a good fitting result.

As can be seen from Table 1, except for the case of the Zn-10 g L⁻¹ TiO₂ (AA) coating, the corrosion potential values of the composite layers are less negative than the one corresponding to the zinc deposit, indicating that the Zn–TiO₂ coatings are less active than pure zinc surface. Moreover, the decreases of the corrosion current density in the presence of the TiO₂ particles, as compared to the i_{corr} value calculated for pure zinc deposit, could be associated to an increase of corrosion resistance of the composite coatings as a consequence of the inclusion of TiO₂ (D or AA) in the metallic deposit. In other words, TiO₂ particles present on the coating surface act as uniform passive sites reducing the corrosion propensity of the coating. The results are in agreement with those reported in the literature [15, 16].

In the case of Zn-10 g L⁻¹ TiO₂ (AA) coating, the higher i_{corr} values and the shift of E_{corr} towards a more negative potential could suggest an acceleration of the corrosion process, probably due to defects and dislocations or to chemical heterogeneities generated in the metallic matrix by the embedded particles [17].

It is worth mentioning that by using the same concentrations of TiO₂ nanoparticles in the plating baths having various crystalline structures and origins (Degussa, Alfa Aesar), different kinetic parameters were obtained. This could be due to the different crystalline structure of the nanoparticles (TiO₂ D is a mixture of anatase, rutile, while TiO₂ AA consists only of anatase) and probably to the different surface properties of the nanoparticles (charge, hydrophobicity, previous treatments etc.). These characteristics certainly play an essential role in their incorporation mechanism and may influence the corrosion behavior of the resulting coatings. A dependence of the incorporation fraction on the crystalline structure of the nanoparticles was already reported for other composites such as Ni–TiO₂ [2, 18, 19].

The values of the anodic and cathodic Tafel coefficients calculated for the Zn–TiO₂ composite coatings change in comparison with those for the pure zinc deposit, indicating that the embedded TiO₂ nanoparticles influence the kinetics of both the anodic and cathodic processes.

3.3 Electrochemical impedance spectroscopy

The impedance spectra corresponding to the corrosion of Zn coatings obtained in the absence and in the presence of different TiO₂ (D or AA) nanoparticles exhibit a capacitive behavior with depressed loops, in the whole frequency domain. This behavior is typical and has been explained assuming metal dissolution under a corrosion product film with oxygen reduction within the film pores [20].

Fig. 5 SEM micrographs of the surface of Zn (**a**), and Zn–TiO₂ films prepared with 3 g L⁻¹ (**b**), and 5 g L⁻¹ (**c**), and 10 g L⁻¹ (**d**), Degussa nanoparticles, after 48 h immersion in 0.2 g L⁻¹ (NH₄)₂SO₄ (pH 3) solution

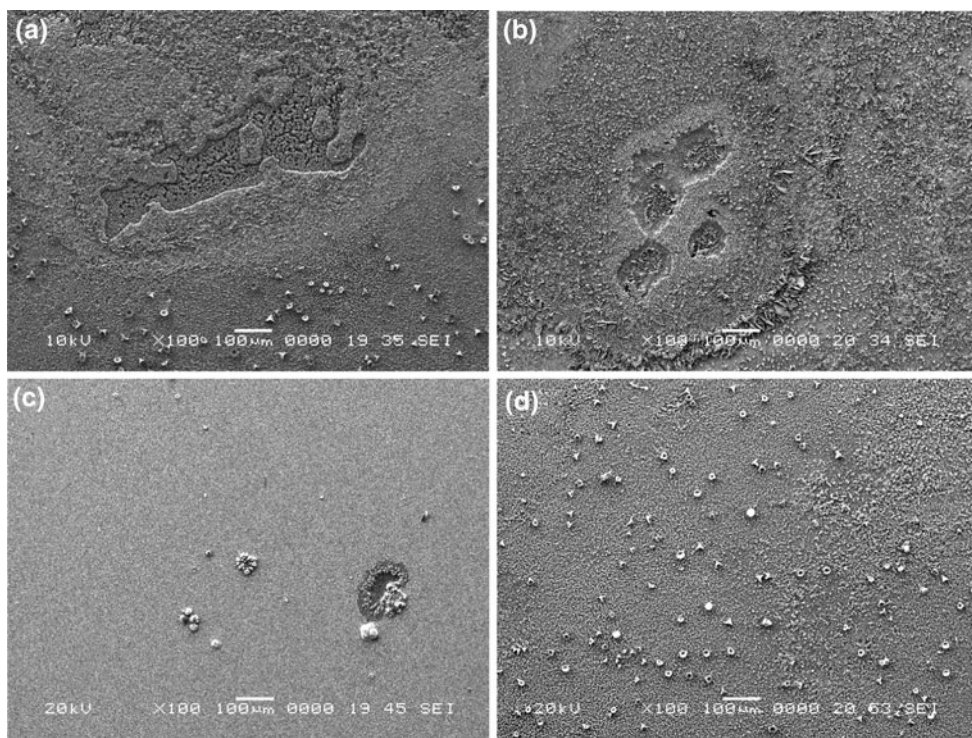


Fig. 6 Polarization curves for pure zinc deposit and for the composite coatings. **a** Zn–TiO₂ (Degussa), **b** Zn–TiO₂ (AA) recorded after 1 h immersion in 0.2 g L⁻¹ (NH₄)₂SO₄ (pH 3) solution

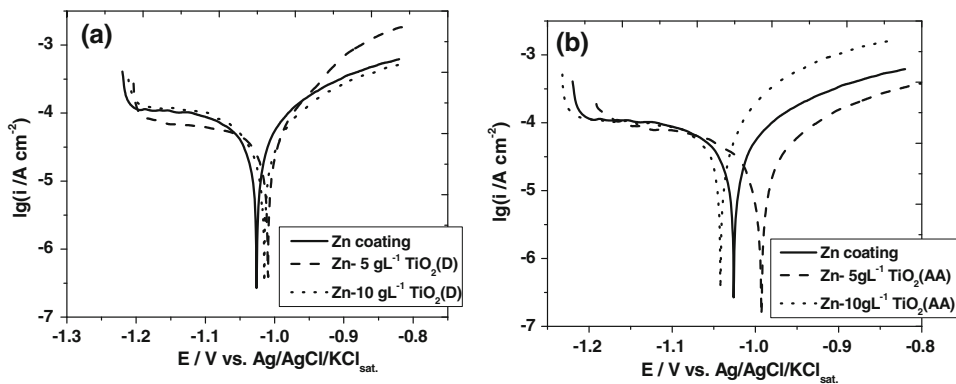


Table 1 Corrosion parameters estimated from potentiodynamic measurements for pure zinc deposit and for Zn–TiO₂ composite coatings obtained with different concentrations of TiO₂ nanoparticles in the plating bath

TiO ₂	TiO ₂ conc. (g L ⁻¹)	E_{corr} (V)	i_{corr} ($\mu\text{A cm}^{-2}$)	b_a (V ⁻¹)	$-b_c$ (V ⁻¹)	R^{2}
–	0	-1.027	110	11.44	4.14	0.9989
Degussa	5	-1.016	40	24.41	7.37	0.9979
	10	-1.018	90	10.95	4.76	0.9979
Alfa aesar	5	-0.999	60	11.19	8.01	0.9959
	10	-1.051	140	14.95	6.84	0.9924

Figure 7 illustrates the evolution of the impedance diagrams for Zn deposit and for different Zn–TiO₂ composite coatings as a function of the immersion time, in 0.2 g L⁻¹ (NH₄)₂SO₄ (pH 3) aqueous solution.

It can be noticed that, except for the case of Zn-10 g L⁻¹ TiO₂ (AA) coating, in the first moments after the

immersion in the corrosive media, the impedance modulus of the Zn–TiO₂ coatings is higher than the impedance values corresponding to the pure Zn deposit and it significantly increases with the immersion time.

Three capacitive loops are necessary for computer fitting of experimental data with an electrical equivalent circuit.

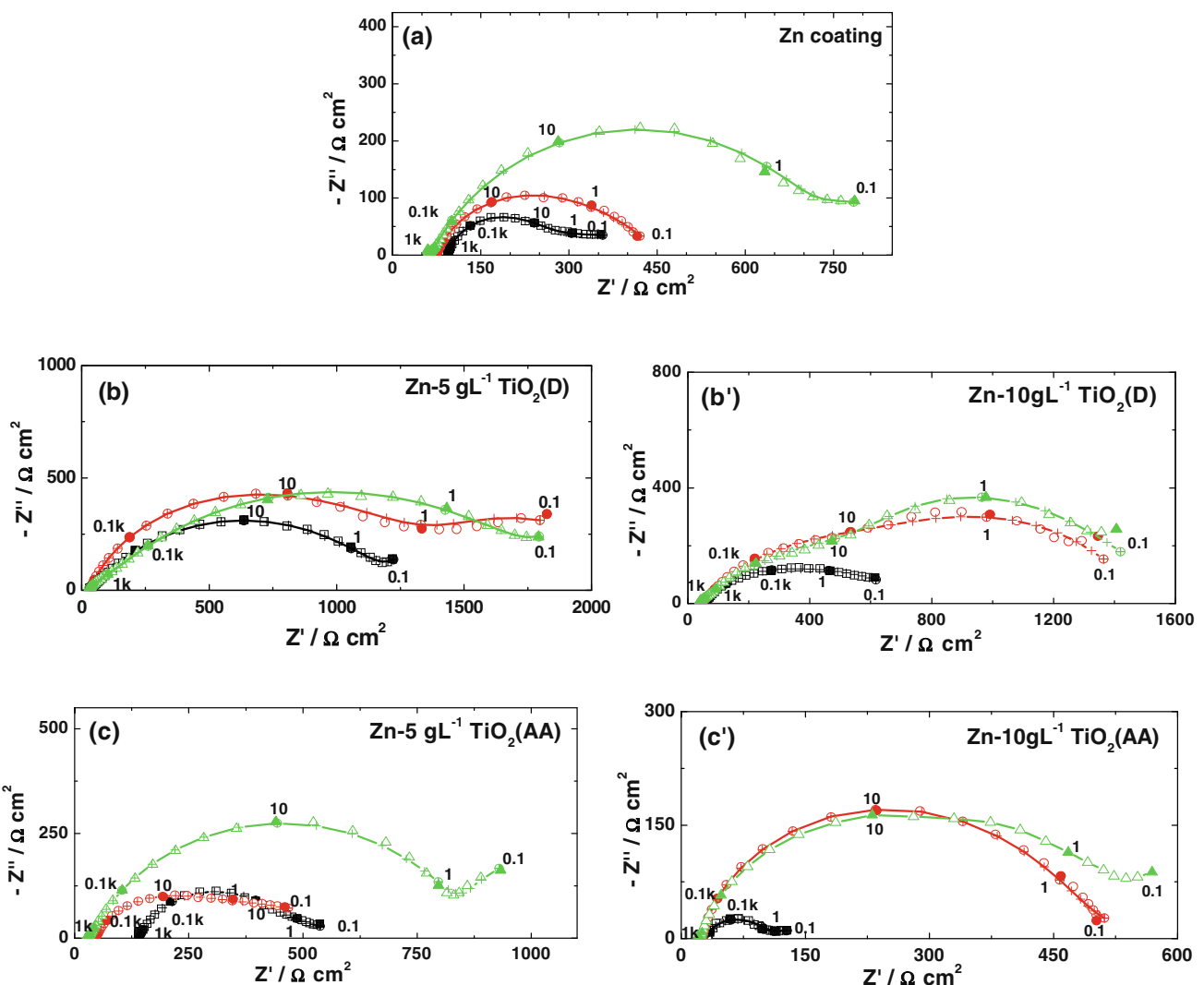


Fig. 7 EIS evolution of pure zinc deposit (**a**), and of the composite coatings: Zn-TiO₂ (Degussa) (**b**, **b'**), Zn-TiO₂ (AA) (**c**, **c'**) immersed in 0.2 g L⁻¹ (NH₄)₂SO₄ (pH 3) corrosive solution, after various

The (3RC) electrical circuit presented in Fig. 8 was therefore adopted to carry out a non-linear regression calculation with a Simplex method.

The ($R-C$) couples used in the equivalent circuit from Fig. 8 could be ascribed to the following contributions [21]:

- The high frequency elements ($R_f - C_f$) are related to the dielectric character of the corrosion products (C_f) due to formation of a thin surface layer that is reinforced by the ionic conduction through its pores (R_f);
- The medium frequency contribution ($R_t - C_d$) is attributed to the double layer capacitance (C_d) at the zinc electrolyte interface at the bottom of the pores coupled with the charge transfer resistance (R_t);

immersion times: square 1 h, circle 24 h and triangle 48 h. The symbol plus corresponds to the fitted data. Frequencies are expressed in Hz

- The low frequency contribution ($R_F - C_F$) is ascribed to the redox process taking place at the electrode surface, probable involving the corrosion products layers accumulated at the interface.
- n_d , n_f , and n_F are coefficients representing the depressed characteristic of the capacitive loops in the Nyquist diagrams.

A capacitive loop was calculated according to the following equation [22]:

$$Z = \frac{R}{1 + (j \cdot \omega \cdot R \cdot C)^n} \quad (2)$$

From this equation with distribution of time constant by n , C has the dimension of F cm⁻², and corresponds to the value at the frequency of the apex in Nyquist diagram.

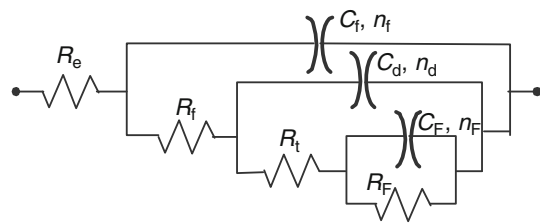


Fig. 8 The (3RC) equivalent electrical circuit used for computer fitting of the experimental data

As can be seen from the comparison of the experimental with the calculated impedance spectra presented in Fig. 7, the (3RC) equivalent electrical circuit reproduce suitably the experimental data corresponding to the zinc coatings obtained in the absence and in the presence of different TiO_2 (D or AA) nanoparticles.

The values of the impedance parameters calculated by non-linear regression of the impedance data for Zn deposit and for Zn– TiO_2 composite coatings obtained with different concentrations of TiO_2 nanoparticles (D and AA) in the plating bath are presented in Table 2.

In most cases, the R_f values are larger in the presence of TiO_2 nanoparticles than in their absence, whereas the C_f values decrease suggesting that the layer of corrosion products formed on the Zn– TiO_2 coatings (probably involving ZnO , an hydrated zinc hydroxyl-sulfate $\text{ZnSO}_4 \cdot y(\text{OH})_2 \cdot n\text{H}_2\text{O}$ [23–26]) is probably thicker and less permeable than in the absence of the embedded nanoparticles.

Furthermore, for the composite coatings incorporating TiO_2 , the charge transfer resistance, R_t increases, while the double layer capacitance decreases as compared with the values obtained for pure Zn deposit. The decreases of the

C_d values in the case of the composite coatings could be attributed to a decrease of the active area directly in contact with the corrosive media as a consequence of the incorporation of TiO_2 in Zn deposit, or to an increase in the thickness of the corrosion products formed on the surface [27]. This tendency was found in accordance with other data reported in the literature [5] for Zn– TiO_2 composites.

The variations of the R_F and C_F values point to a development of the corrosion products layer formed during the long-time measurements.

The increase of corrosion resistance during long-term measurements suggests that a barrier related to the formation of corrosion products gradually forms on the zinc surface. This phenomenon has been observed both in the case of pure Zn deposit and in the case of Zn– TiO_2 composite coatings, indicating an evolution of the corrosion products layer in time. The formation of a corrosion products layer has a protective effect against corrosion by progressively displacing the rest potential and by increasing the transfer resistance. However, this layer tends to be eliminated by potential activation or by zinc dissolution. This competition is time dependent and explains why the electrochemical behavior of zinc is often considered as poorly reproducible, especially in the vicinity of the rest potential [25].

In the case of $\text{Zn-10 g L}^{-1} \text{ TiO}_2$ (AA) coating, the significant decrease of R_t and R_F values observed in the first moments after the sample immersion in the corrosive solution indicates an acceleration of the corrosion rate and also, an increase of the reactivity of the surface corrosion products. This observation is in accordance with the results obtained from the polarization measurements and could be

Table 2 Parameter values for Zn and Zn– TiO_2 coatings corrosion calculated by non-linear regression of the impedance data using the (3RC) equivalent electrical circuit

TiO_2	TiO ₂ conc. (g L^{-1})	Time (h)	R_e ($\Omega \text{ cm}^2$)	R_f ($\Omega \text{ cm}^2$)	C_f ($\mu\text{F cm}^{-2}$)	R_t ($\Omega \text{ cm}^2$)	C_d ($\mu\text{F cm}^{-2}$)	R_F ($\Omega \text{ cm}^2$)	C_F (mF cm^{-2})	R_p^a ($\Omega \text{ cm}^2$)
Degussa	0	1	93.83	77.72	15.94	249.41	400	90	3.38	417.13
		24	74.95	120.54	72.46	300.98	182.1	134.70	1.20	556.22
		48	64.34	159.00	17.31	493.08	17.15	175.14	9.17	827.22
	5	1	26.00	143.50	1.57	980.90	1.80	323.55	17.05	1447.95
		24	33.16	160.77	3.34	1474.80	3.91	612.81	1.43	2248.38
		48	22.37	237.95	1.66	1503.90	4.80	708.85	19.98	2450.70
Alfa aesar	10	1	51.07	120.29	11.01	422.56	23.65	266.76	0.58	809.61
		24	42.88	170.79	2.20	650.00	3.65	658.87	0.18	1479.66
		48	37.01	232.70	0.6	767.34	1.56	707.64	0.11	1707.68
	5	1	140.29	159.00	9.91	306.95	22.29	152.85	1.13	618.80
		24	45.36	35.57	2.82	479.01	4.64	256.68	0.89	771.26
		48	27.19	32.29	2.67	822.58	4.03	358.46	8.95	1213.33
	10	1	21.65	16.65	2.08	73.16	13.66	42.01	53.66	131.82
		24	16.46	20.26	2.97	390.28	21.08	146.61	1.01	557.15

^a $R_p = R_f + R_t + R_F$

correlated with a non-uniform distribution or an agglomeration of the TiO_2 nanoparticles in the $\text{Zn-10 g L}^{-1} \text{TiO}_2$ (AA) deposit. In the aqueous plating bath, particles easily agglomerate due to the compression of the diffuse double layer surrounding the particles by their high ionic strength. Consequently, the anticipated mechanical, chemical and/or physical properties of the composite coatings are not achieved and an enhancement of the corrosion process takes place [28]. This is in accordance with the fact that the corrosion resistance depends not only on the incorporation fraction of oxide nanoparticles, but mostly on their uniform distribution in the metallic deposit [29].

The values of the polarisation resistance R_p , calculated as the sum $R_f + R_t + R_F$ from the resistances values determined by the regression calculation (Table 2) reveal that, apart from the case of $\text{Zn-10 g L}^{-1} \text{TiO}_2$ (AA) coating, the corrosion rate significantly decreases in the presence of both types of TiO_2 nanoparticles. This effect could be related to the reduction of the active surface of the coating in contact with the aggressive environment, due to the presence of embedded TiO_2 nanoparticles [4]. R_p is the highest in the case of the $\text{Zn-5 g L}^{-1} \text{TiO}_2$ (D) composite coatings.

4 Conclusions

In the same experimental conditions, TiO_2 Degussa incorporates better and confers superior corrosion protection to zinc coatings than TiO_2 Alfa Aesar, probably because of the different size, crystalline structure and surface properties of the nanoparticles. This result confirms once again the important relationship between the particles characteristics and their incorporation rate, evidenced also in other cases [30].

The highest polarization resistance, R_p , indicating the best corrosion protection, was observed in the case of the composite coatings $\text{Zn-5 g L}^{-1} \text{TiO}_2$ (D), which is in agreement with the results obtained from polarisation measurements and during the morpho-structural analysis of the coatings. The existence of an optimal concentration of TiO_2 in the plating bath (5 g L^{-1} for TiO_2 Degussa) could be explained by the fact that the corrosion resistance of the resulting Zn-TiO_2 coatings is eventually determined by two contrary effects: on one side, the embedded inert oxide particles diminish the active surface in contact with the corrosive environment and, on the other side, they disturb the electrocrystallization process, by generating dislocations and defects in the metallic matrix which act as chemical heterogeneities and favor the corrosion process [31].

In the case of $\text{Zn-10 g L}^{-1} \text{TiO}_2$ (AA) coating, the poorer corrosion resistance could be due to a non-uniform distribution of TiO_2 (AA) nanoparticles in the Zn matrix as a consequence of their agglomeration in the electrolyte.

This behavior is consistent with the higher corrosion current densities observed on the polarization curves and with SEM observations.

Acknowledgments The financial support within the project PN II INOVARE No. 97/28.09.2007 (NANOTECH) is gratefully acknowledged. The authors thank Mr. Florin Popa, from UTCN Cluj-Napoca, for the SEM-EDX analyses.

References

- Kondo K, Ohgishi A, Tanaka Z (2000) J Electrochem Soc 147:2611
- Low CTJ, Wills RGA, Walsh FC (2006) Surf Coat Technol 201:371
- Tuaweri TJ, Wilcox GD (2006) Surf Coat Technol 200:5921
- Gomes A, Da Silva Pereira MI, Mendonça MH, Costa FM (2005) J Solid State Electrochem 9:190
- Praveen BM, Venkatesha TV (2008) Appl Surf Sci 254:2418
- Deguchi T, Imai K, Matsui H, Iwasaki M, Tada H, Ito S (2001) J Mater Sci 36:4723
- Mukherjee D, Palaniswamy N, Guruviah S, Belthowska E, Barbara P (1990) Bull Electrochem 6:380
- Satoshi O, Hiroaki N, Shigeo K, Tetsuya A, Hisaaki F, Kazuo O (2002) J Surf Finish Soc Japan 53:920
- Mokshanatha PB, Venkatarangaiah VT, Arthoba NY, Kalappa P (2007) Metal-Org Nano-Metal Chem 37:461
- Muresan L, Gherman M, Zamblau I, Varvara S, Bulea C (2007) Stud Univ Babes-Bolyai Chem LII:97
- Guglielmi N (1972) J Electrochem Soc 119:1009
- Abdel Hamid Z (2001) Anticorros Methods Mater 48:235
- Fustes J, Gomes A, Da Silva Pereira MI (2008) J Solid State Electrochem 12:1435
- Stern M, Geary AL (1957) J Electrochem Soc 104:56
- Mukherjee D, Venkataraman B, Palaniswamy N, Natesan M, Balakrishnan K (1987) Key Eng Mater 20–28:3689
- Shibli SMA, Dilimov VS, Smith PA, Manu R (2006) Surface Coat Technol 200:4791
- Vlasa A, Pop AV, Varvara S, Chira M, Bulea C, Muresan L (2009) Optoelectron Adv M Rapid Communications 3:1290
- Celis JP, Roos JR (1983) Oberfl-Surf 24:352
- Li J, Sun Y, Sun X, Qiao J (2005) Surf Coat Technol 192:331
- Juettner K, Lorenz WJ, Kendig MW, Mansfeld F (1988) J Electrochem Soc 135:332
- Dermaj A, Hajjaji N, Joiret S, Rahmouni K, Srhiri A, Takenouti H, Vivier V (2007) Electrochim Acta 52:4654
- Muresan L, Varvara S, Stupnisek-Lisac E, Otmacic H, Marusic K, Horvat-Kurbegovic S, Robbiola L, Rahmouni K, Takenouti H (2007) Electrochim Acta 52:7770
- Magainoa S, Soga M, Sobue K, Kawaguchi A, Ishida N, Imai H (1999) Electrochim Acta 44:4307
- Chung SC, Sung SL, Hsien CC, Shih HC (2000) J Appl Electrochem 30:607
- Cachet C, Ganne F, Maurin G, Petitjean J, Vivier V, Wiart R (2001) Electrochim Acta 47:509
- Barranco V, Feliu S Jr, Feliu S (2004) Corros Sci 46:2203
- Santana Rodriguez JJ, Motesdeoca Alvarez C, Gonzalez Gonzalez JE (2006) Mater Corros 57:350
- Lozano-Morales A, Podlaha EJ (2004) J Electrochem Soc 151:C478
- Fontenay F, Andersen LB, Moller P (2001) Galvanotechnik 92:928
- Maurin G, Lavanant A (1995) J Appl Electrochem 25:113
- Hovestad A, Jansen LJJ (1995) J Appl Electrochem 25:519